JOURNAL OF MATERIALS SCIENCE **39** (2004) 5995–6003

Carbon fiber reinforced hafnium carbide composite

A. SAYIR
NASA Glenn Research Center/Case Western Reserve University, Cleveland, OH 44135, USA
E-mail: Ali.Sayir@grc.nasa.gov

Hafnium carbide is proposed as a structural material for aerospace applications at *ultra high* temperatures. The chemical vapor deposition technique was used as a method to produce monolithic hafnium carbide (HfC) and tantalum carbide (TaC). The microstructure of HfC and TaC were studied using analytical techniques. The addition of tantalum carbide (TaC) in the HfC matrix was studied to improve the microstructure. The microstructure of HfC, TaC and co-deposited hafnium carbide-tantalum carbide (HfC/TaC) were comparable and consisted of large columnar grains. Two major problems associated with HfC, TaC, and HfC/TaC as a monolithic are lack of damage tolerance (toughness) and insufficient strength at very high temperatures. A carbon fiber reinforced HfC matrix composite has been developed to promote graceful failure using a pyrolytic graphite interface between the reinforcement and the matrix. The advantages of using carbon fiber reinforcement with a pyrolytic graphite interface are reflected in superior strain capability reaching up to 2%. The tensile strength of the composite was 26 MPa and needs further improvement. Heat treatment of the composite showed that HfC did not undergo any phase transformations and that the phases comprising composite were are thermochemically compatible.

1. Introduction

Expandable and reusable space vehicles, next generation rocket engines and hypersonic spacecraft need materials and structural components capable of operating at temperatures in excess of 1600°C. The ultimate payoff is expected to come when materials are developed that can perform without cooling at gas temperatures exceeding 2200°C. Temperatures above 1600°C, and if possible exceeding 2200°C, will be described as the *ultra high* temperature region to differentiate the unique thermomechanical and thermochemical demands of aerospace applications. Materials for rocket combustion chambers, thrusters, and nozzles must meet several requirements simultaneously, such as high melting temperature, minimum strength, and environmental resistance (i.e., oxidation resistance).

The selection of potentially suitable structural materials for use at *ultra high* temperatures in air breathing engines was identified in reports by the Air Force Wright Aeronautical Laboratories [1–6]. Borides, carbides, boride-graphite composites, carbide-graphite composites, pyrolytic and bulk graphite, coated refractory metals/alloys, oxide-metal composites, oxidation resistant refractory metal alloys, oxide-metal composites, and iridium-coated graphite were considered for *ultra high* temperature applications (see Table I). Boride composites were developed at Air Force Laboratory for leading edge and nose cap applications which require moderately high temperatures. Several other researchers proposed monolithic ZrB_2 [7–9] and HfB_2 [7, 8, 10], as well as and composites of these boride materials with other ceramics, including TiC/ZrB_2, TiC/HfB_2, SiB_6/ZrB_2, [8], and ZrB_2/SiC or HfB_2/SiC. A major reason for proposing these materials, however, was the availability of easy fabrication through hot pressing, resulting in high relative density and a concomitant high strength. The oxidation resistance of these materials was limited [11–15]. A renewed effort to fabricate HfB_2-SiC and ZrB_2-SiC composites is underway to tackle the challenges related to oxidation that exist for *ultra high* temperature region [16–18]. Still, the development of processing technology to produce near-net shape components is a formidable task.

A second group of important materials for aerospace applications is based on monolithic refractory metal and refractory metal based composites [19]. These materials are of interest for their high strength and ductility at elevated temperatures. Some of these materials should be capable of carrying significant loads at *ultra high* temperatures, but they have the disadvantage of very low specific strength. Engine weight and inertial force considerations often put a premium on utilizing materials with low density. Hence, the mechanical requirements, such as strength, stiffness, and creep resistance have to be normalized with respect to density. In rotating or reciprocating machines, and especially in structures to be air- or space borne, these density-normalized properties become the criteria of interest. From the point-of-view of specific strength requirements the metals listed in Table I (W, Mo, Ir,

TABLE I Classification of materials using single criteria; melting point [1–10, 20–22]

Type of material	Prime materials $T_m > 3000^\circ C$	Marginal materials $T_m \ll 3000^\circ C$
Carbon	Diamond, graphite	
Metals	W, Mo, Ir, Os, Ta	
Intermetallics		ReW, Re_3W, Re_2Ti_5,
Light Ceramics		SiC, B_3Si
Refractory metal Ceramics	HfC, TaC, NbC, ZrC, Ta_2C, TiC, HfN, TaN, HfB, HfB_2, TaB_2, ZrB_2,NbB_2, ThO_2	WC, W_2C, VC,MoC, Mo_2C, ZrN, TiN, WB, TiB_2, Nb_3B_4, WB_2, YB_2, ZrB, W_2B, HfO_2, UO_2, $ThZrO_4$, MgO, ZrO_2-Er_2O_3, ZrO_2, $SrZrO_3$

Os and Ta) are not satisfactory. These metals, W, Mo, Os and Ta, also have very poor oxidation resistance. Iridium and compatible alloys perform admirably for rocket throat and nozzle applications [20–22], but high density, high cost of raw materials, and laborious machining operations makes iridium and its alloys less attractive.

A third group of candidate materials is based on high temperature carbides and nitrides. In *ultra high* environments such as that of rocket engines, structural components must be capable of withstanding shock and high structural loads in highly corrosive environments. A material therefore should not undergo any significant surface degradation in high temperature oxidizing environments. This requirement eliminates from consideration all materials that react with oxygen to form volatile products. The volatility can be quantified in terms of vapor pressure and oxidation-induced surface recession rates as a function of temperature. Shaw *et al.* [23], Wicks *et al.* [24] and Shick *et al.* [25] have shown that the carbides tend to have lower pressures than borides and nitrides.

Using the volatility data from Shaw *et al.* [23], one can conclude that HfC is one of the candidate materials for use in *ultra high* temperature environments. Another primary requirement of a candidate material is low diffusion coefficients at high temperatures. The material should be stable with respect to chemical interactions with the oxidation product, as well as any secondary phases present, over long periods at elevated temperatures. These objectives can be met by selecting materials that possess large negative free energies of formation. Hafnium carbide fulfills these thermodynamic requirements and it is the choice of material for this investigation. Another justification for the selection of HfC is derived from the mode of oxidation of HfC to HfO_2. During oxidation of hafnium carbide, a very distinctive and heterogeneous structure forms that has important implications in potential applications [26–30]. The structure contains three distinct layers: (a) a residual carbide layer with dissolved oxygen in the lattice, (b) a dense oxide interlayer containing carbon (HfC_xO_y), and (c) a porous outer layer of hafnium oxide. Bargeron *et al.* [31] has shown that the interlayer HfC_xO_y has remarkably low diffusion coefficient ($D_{i,eff} = 1.1 \times 10^{-7}$ cm^2/s at 2060°C) and is an oxygen diffusion barrier.

Although chemically stable at high temperatures, HfC would require fiber reinforcement to attain strain-to-failure capability (increased toughness) suitable in load-bearing applications. High strength carbon fibers are currently the only suitable reinforcement for the composites used at *ultra high* temperatures. Carbon fibers can readily be formed into a construct or perform of desired configuration by winding, weaving, knitting, braiding, or wrapping over a suitably formed mandrel. In addition, carbon fibers are relatively inexpensive. A composite of hafnium carbide as the matrix and carbon fibers as the reinforcement emerges as the candidate material having the highest upper use temperature. The aim of this work was to produce carbon fiber-reinforced hafnium carbide (HfC) composites and study the microstructure—mechanical property relationship. The goal is to produce a strong and tough composite that will withstand an operating temperature of 2200°C but for short time applications (minutes rather than hours). The HfC matrix was produced via chemical vapor deposition (CVD). This method provides a high degree of control of deposition rates and is capable of producing complex shaped components with superior uniformity.

2. Experimental

Pyrolytic graphite, HfC, TaC, and HfC/TaC were deposited by CVD on different substrates by Advanced Ceramics Corporation (ACC)[1]. The CVD process was carried out using an industrial-scale furnace which consisted of a graphite susceptor, insulation jacket, and induction coil which were contained within a water-jacketed steel vacuum shell that could be evacuated by a vacuum pumping system. It is significant to point out that geometrical parameters play a dominant role in CVD processes and thus, the materials produced in this study would be most comparable to other materials produced by industrial-scale operations. The CVD processing conditions of carbide deposition were proprietary information of ACC and the study of processing conditions was beyond the scope of the present investigation.

Graphite and two dimensional (2D) square-weave carbon fabric (trade name WCA graphite cloth produced with Rayon fibers) were supplied by POCO Graphite Inc., and Morgan Specialty Graphite, respectively. The graphite cloths consisted 10 strands per centimeter and had tensile strength of 150 MPa. Pyrolytic graphite was deposited as an interfacial layer between the carbide (HfC, TaC, or HfC/TaC). It was possible to produce C_{fiber}/HfC_{matrix} composites with complex shape. Wrapping woven carbon fiber cloth over a suitably formed support or mandrel produced the complex shape. Two-dimensional (2D) woven carbon fabrics were coated with 5 to 120 μm thick layers of pyrolythic graphite (PG) on various graphite mandrels. There were several reasons for the deposition of PG on 2D woven carbon fabric. This process rigidized the fabric, thereby

[1]1197 Lakewood, Ohio (Now GE Advanced Ceramics, Strongsville, Ohio).

producing components that could be handled conveniently without bending of the woven carbon-fiber fabric and which retained the shape of the mandrel. The rigidization of fiber fabric through PG deposition had a profound effect on the mechanical properties of the composite, as discussed later. The PG interface layer (5 μm) protected fibers from the reaction with the HfC matrix, thus minimizing fiber strength degradation during processing. PG interface resulted in porous HfC or TaC layer between dense HfC or TaC matrix. Additionally, stereological characterization suggests that the composite was approximately 60% dense.

The processing of complex-shaped structures, however, produced unattractive tensile specimens, which had curvatures. Ribbons of approximately 1×10 mm cross-sections and 20 cm in lengths were machined from these composites with complex shape and curved sections. Tensile strength data were collected using these specimens, although they had an undesirable and inhomogeneous stress state. The assignment of the stress values was estimated from cross-section measurements and did not take into account the torsion and bending forces during the test. The primary intent here was to have a good engineering estimate of the strain capacity of the composite.

Accurate axial strain measurements were used to assess the performance of the composite, specifically the strain-to-failure capability. In contrast to the stress measurements, the strain measurement in axial direction was very accurate. For the tensile tests, cold grips were used with a total gauge length of approximately 40 mm. All samples fractured within the 40 mm gauge length. The strain rates were calculated from the total gauge length and crosshead speed of the test frame (Model 4502, Instron Corp., Canton, MA). A computer controlled digital extensometer (Universal Dimension Meter; UDM500A from Zimmer Corporation) was used to measure the extension. The universal dimension meter (UDM) is specifically designed for precision strain measurements and uses a Mercury Xenon illuminator with suitable collimating lens that illuminates the sample from behind. Flags of silicon carbide monofilaments (SCS6/Textron Corporation) were attached to the sample in order to provide a contrasting edge. The distance between the flags was the gauge length and it was measured with a micrometer. The UDM measures edge positions without contact using a digital line scan method. Its resolution is 5000 pixels at a scan rate of 1800 Hz. The strain measurement system was ASTM83-92 Class A. The measurement error of strain was less than 2% at 25 mm gauge length and expected to be lower at longer gauge lengths. The resolution was 0.25 μm with a maximal sampling rate of 1000 Hz.

X-ray diffraction analysis was carried out using a two-dimensional (2D) General Area Detector Diffraction System, GADDS, manufactured by Bruker AXS, Inc (formerly Siemens AXS). It is a true proton counter in a large area and has a fast rate of data collection. For example, the speed of data collection with an area detector can be 10^4 times faster than with a point detector and about 100 times faster than linear position-sensitive detector. Phase identification has been done by integrating over a selected range of the Bragg angle (2Θ) and the azimutal-angle (χ) about the direction of the incident X-ray beam. The GADDS is also equipped with special flat graphite based rotating-optics monochromators, which produce the strongest beam intensity. The graphite monochromators cannot, however, resolve $K_{\alpha1}$ and $K_{\alpha2}$ lines. Hence, the system was aligned to K_α line to accomplish maximum intensity. The focal spot and critical angle are important features of the system. A 0.8 mm collimator at 13° take off angle with a $1\times$ 10 mm focal spot size at the anode generates the maximum targeting load and brightness. The GADD system operates with a Siemens Kristalloflex 760 X-ray generator which was set at 40 KV and 40 mA and remained stable during the course of this study. Scanning electron microscopy (Joel 840, UTW Kevex EDS) was employed to characterize microstructures and to identify phases.

3. Results and discussion

Initial CVD trials were conducted to investigate the microstructures of HfC and TaC samples deposited on POCO graphite and pyrolytic graphite (PG) substrates. SEM analysis indicated that the microstructures for both POCO graphite and PG substrates were similar and remaining of the work was completed using PG substrates. Figures 1 and 2 are representative SEM micrographs of HfC and TaC samples, respectively. The SEM analysis indicated that both HfC and TaC had a gradually changing structure and had thicknesses of 120 and 30 μm, respectively. HfC contained some voids (Fig. 1a) and the microstructure was void-free as thickness of the coating increased to 30 μm, Fig. 1b. TaC did not contain any void and cracks even though the sample had to be machined and polished extensively to reveal the microstructure, Fig. 2.

The CVD-deposited material tends to grow in a columnar structure. Although the strength of the individual grains may be high, the intergranular strengths can be quite low due to poor cohesion at the boundaries [32]. Average grain sizes exceeding 10–15 μm were produced without microcracks. HfC deposition on pyrolytic graphite (PG) nucleates at the grain boundaries of the PG as small and randomly oriented grains and these random nucleation sites produce a considerable amount of spacing between the grains. This transition structure between the PG and HfC was approximately 10 to 20 μm thick porous layer. The structure was independent of the carbide phase, HfC or TaC, that was deposited.

The mixture of hafnium carbide tantalum carbide (HfC/TaC) matrix phase deposited using the same process. Process conditions were selected to produce 4 mol% TaC in the HfC structure. The microstructure of the co-deposited HfC/TaC, including grain size, was similar to HfC (or TaC) microstructures (see Fig. 3). XRD scans of HfC and TaC matched powder diffraction files 39-1491 and 38-1364, respectively. HfC and TaC exhibit very similar X-ray patterns because they have the same cubic cell structure [33, 34] and they have similar lattice parameters (lattice spacings of HfC and TaC

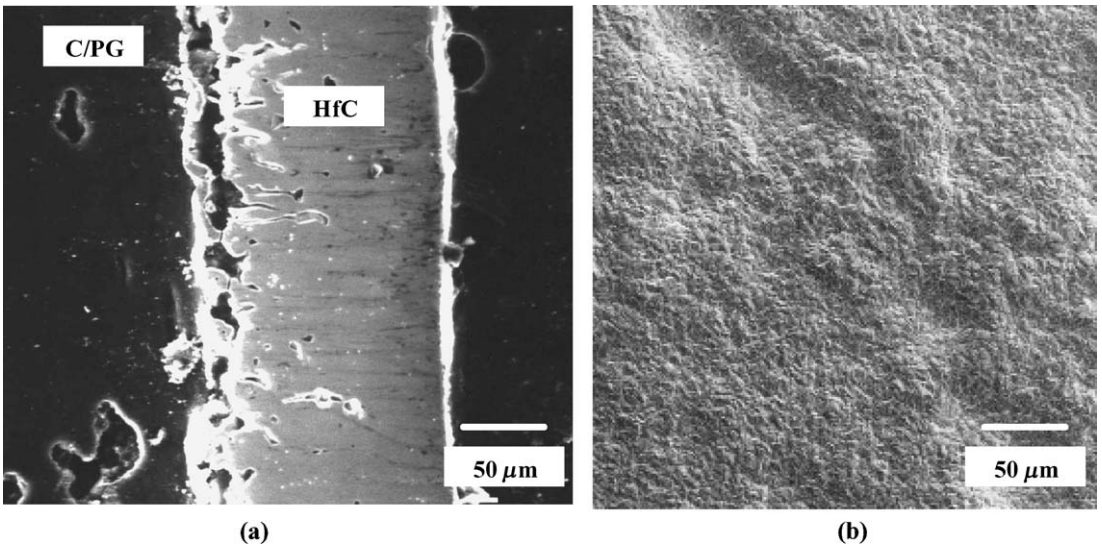

Figure 1 SEM micrograph of thick HfC layer (>120 μm). (a) Columnar growth showing features that are typical for high deposition rates. The compliant transition region between PG and HfC contains voids and enables the growth of a thick HfC layer. (b) Surface morphology of HfC without any void.

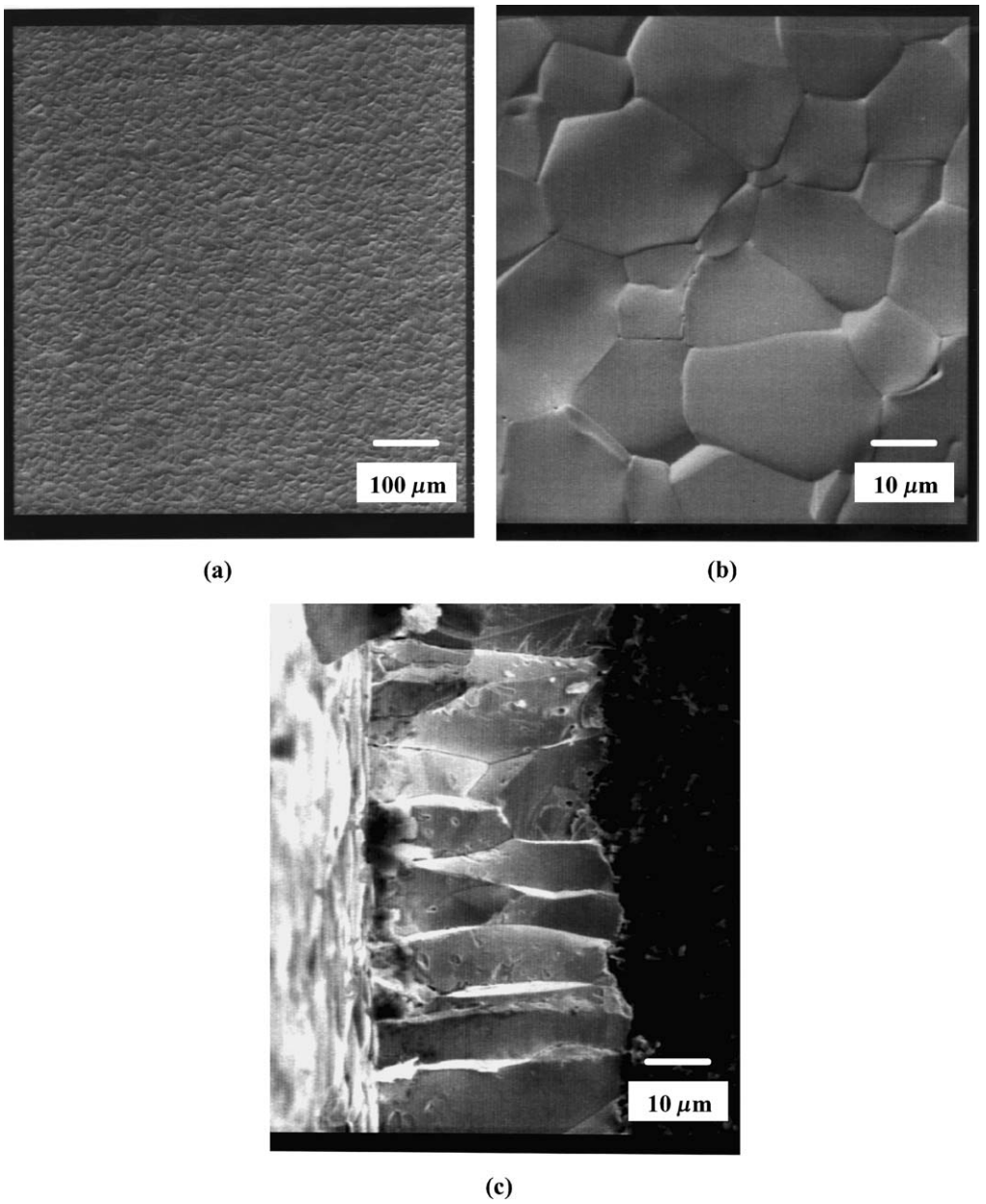

Figure 2 SEM micrograph of as-deposited 30 μm thick TaC coating on Poco ZXF graphite: (a) Surface morphology, (b) Higher magnification, and (c) Fractured edge of TaC coating showing columnar structure.

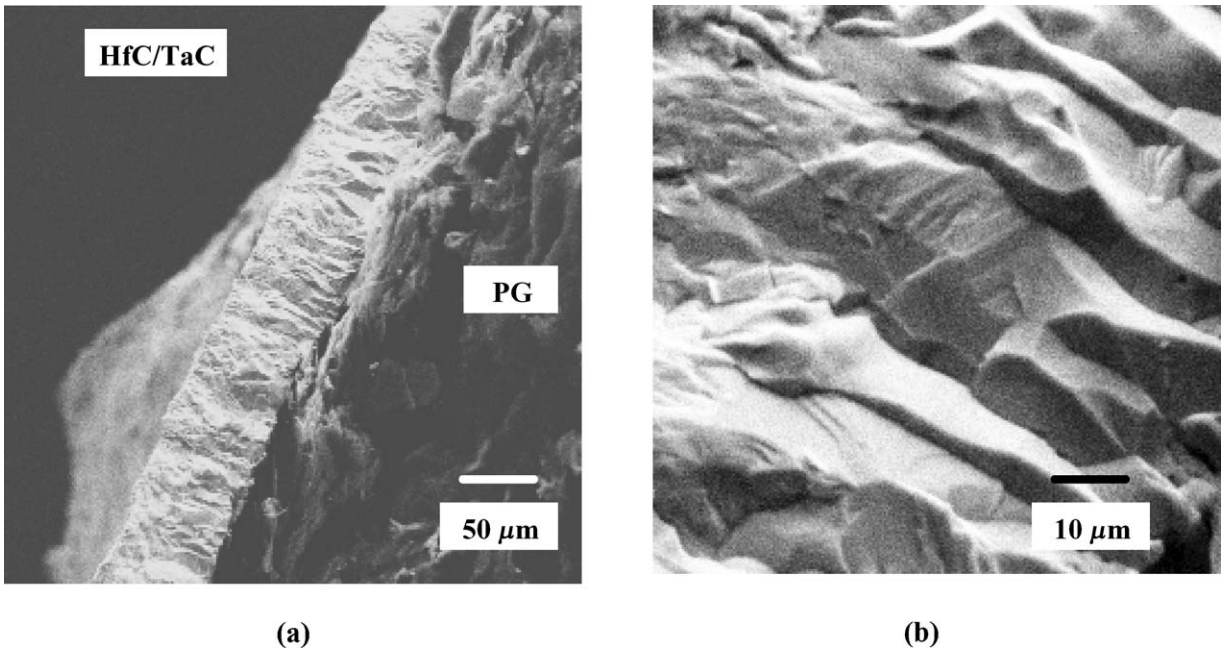

Figure 3 (a) Co-deposited HfC/TaC fracture surface morphology. (b) Higher magnification of the fractured edge showing columnar structure.

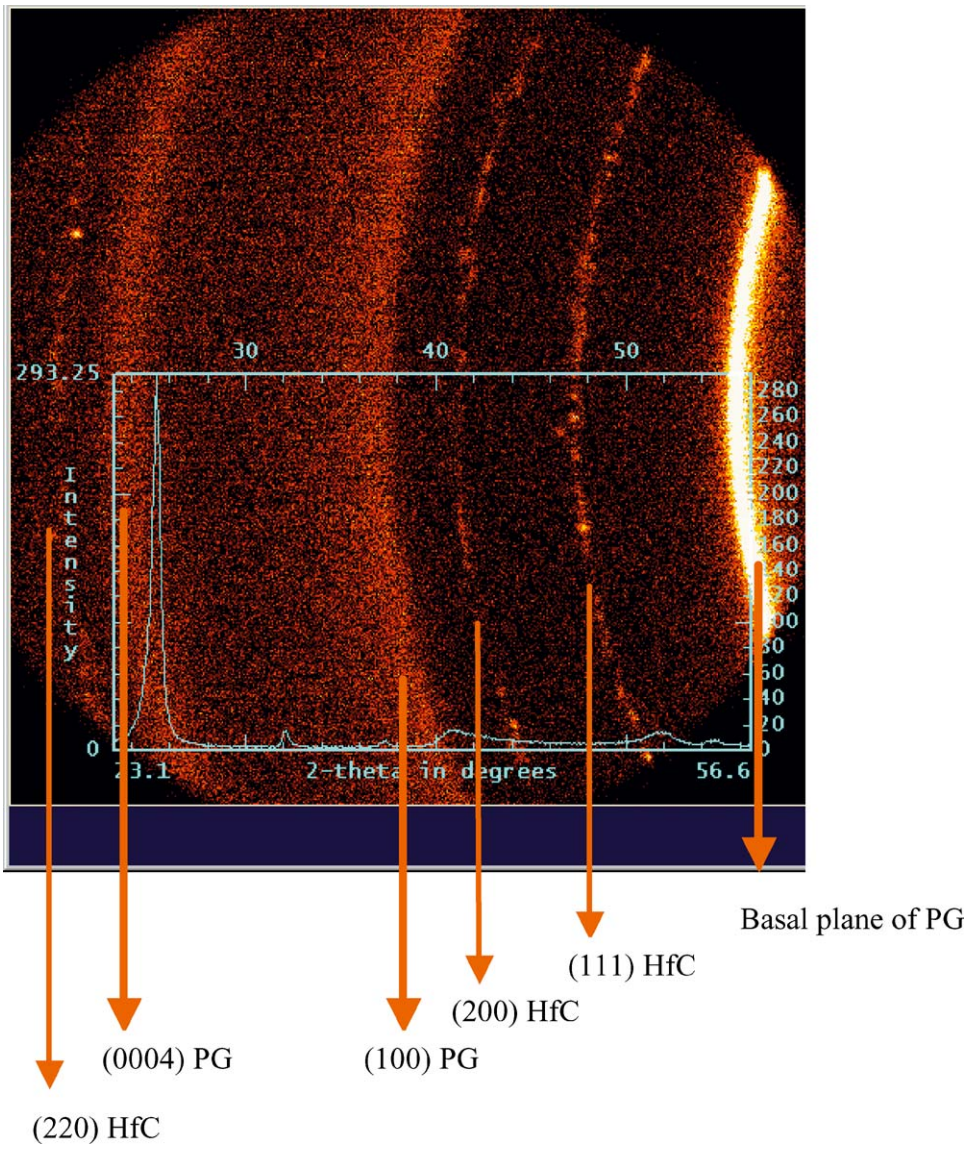

Figure 4 Two-dimensional diffraction pattern of HfC and PG. Large Bragg angle (2Θ) and the azimutal-angle (χ) measured simultaneously. The insert, intensity versus 2Θ, has been obtained by the integration of the data. PG has wide and homogeneous intensity distribution bands (Debye rings). HfC has discontinuously distributed and rather narrow Debye rings.

are 4.64 and 4.0 Å, respectively). The two-dimensional images of X-ray diffracting cones intersecting the area detector revealed much less continuity of the diffraction peak for HfC/TaC indicating slightly finer grain structure. The combination of XRD and SEM analyses indicated that a heterogeneous microstructure consisting of HfC matrix and TaC precipitates was produced. The amount of Ta dissolved in the HfC matrix and quantitative phase amounts of HfC and TaC were not determined. The TaC addition (co-deposition of HfC/TaC) did not reduce the grain size and material development focused on the carbon fiber reinforced HfC matrix.

Figures 4 and 5 reveal some microstructural information concerning a $C_{fiber}/PG_{interface}/HfC_{matrix}$ composite. An extensive SEM analysis on several fibers revealed that the PC coating was very uniformly coated on the

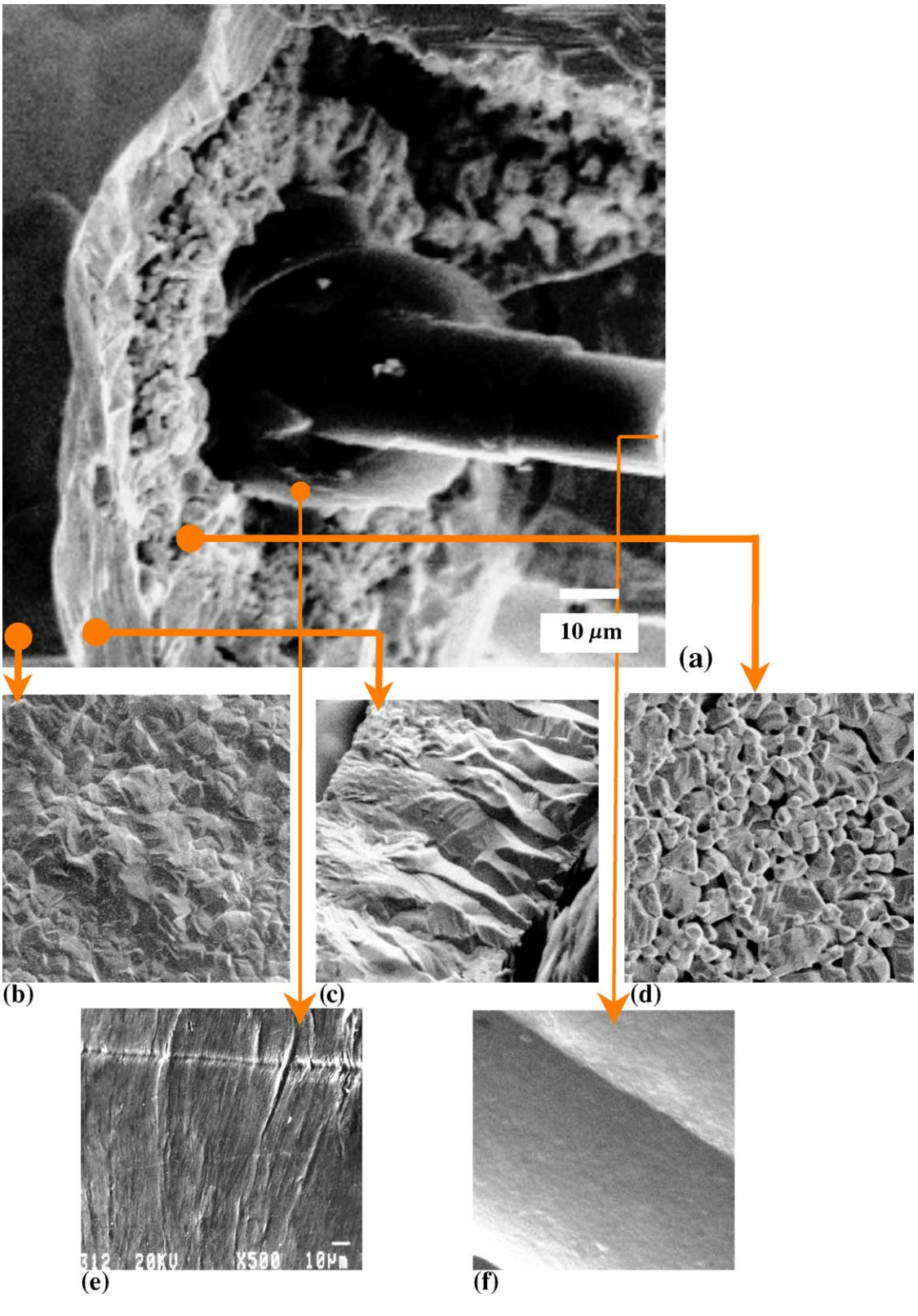

Figure 5 (a) Fracture morphology of $C_{fiber}/PG_{interface}/HfC$ composite. (b) Outer surface morphology of HfC. (c) Columnar structure of HfC, crystal at the start of the growth. (d) Low density HfC layer. (e) PG layer. (f) The edge of fiber fracture surface.

fiber fabrics and had very uniform surface texture. The Debye rings obtained from PG are associated with the basal and prism planes of PG and are homogeneously distributed as large bright bands over the azimutal-angle. Pronounced individual spots with incomplete Debye rings were correlated with the structures shown in composite Fig. 5b, c and d. The nominal PG coating thickness was approximately 5 μm and some composites with 10 μm PG coating was produced around the fibers without bridging to the neighboring fiber. The thick coating of PG was selected to reduce the heat transfer from the exterior to the fibers during ultra high temperature use.

A necessary condition for achieving of high toughness in fiber-reinforced ceramic composites is the promotion of crack deflection and delamination mechanisms. In the present case, this was attained using a low-modulus interface, PG, between the carbon fiber and the HfC matrix. The micrographs in Fig. 5 illustrates the results for $C_{fiber}/PG_{interface}/HfC_{matrix}$ composite produced by different microstructures at different regions of the constituent phases, (fiber, interface and matrix). The nominal volume fraction of the fiber content estimated to be 20 vol%. The woven fiber cloths were coated with PG to achieve a low modulus, laminated interface between the HfC-matrix and the carbon fiber bundles. The deposited PG, however, exhibited high density and a high degree of preferred orientation of the graphite crystallites as determined by texture analysis of X-ray results (representative example is shown Fig. 4) and caused strain due to thermal expansion mismatch between the PG and the HfC. The porous HfC structure, Fig. 5d, between highly textured PG and fully dense HfC matrix was effective to produce a crack free HfC matrix. The bond strength perpendicular to the deposition plane of PG is very low and readily promotes strain energy release through the frictional dissipation of strain energy, thereby producing a high toughness material.

The stress vs. strain behavior of $C_{fiber}/PG_{interface}/HfC_{matrix}$ composites was evaluated in tension. Figures 6 and 7 show stress—strain curves for the samples

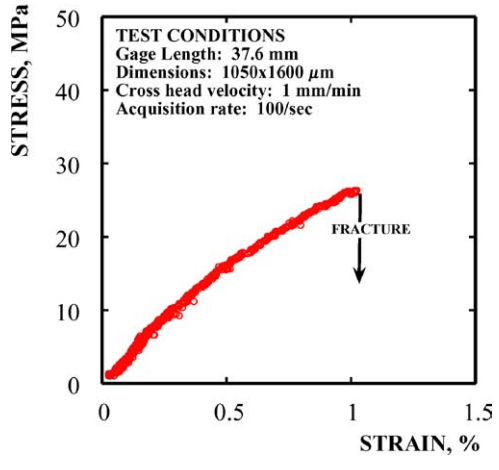

Figure 6 Stress vs. strain behavior of a $C_{fiber}/PG_{interface}/HfC$ composite at room temperature. The test conditions are included in the figure. This represents lowest measured fracture strain capability for a $C_{fiber}/PG_{interface}/HfC$ composite.

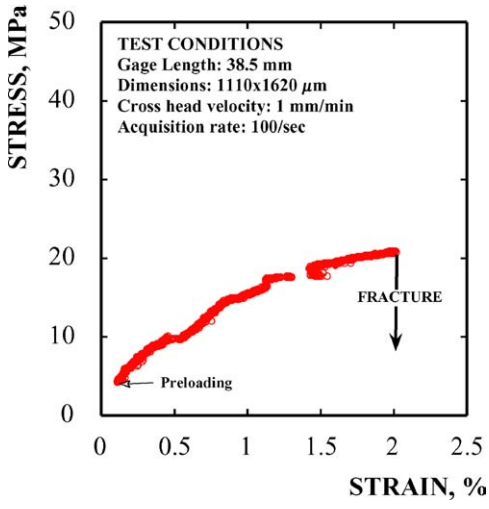

Figure 7 Stress vs. strain behavior of a $C_{fiber}/PG_{interface}/HfC_{matrix}$ composite at room temperature. The test conditions are included in the figure. The graph is representative of a composite with fracture strain (~2%). The interrupted data at ~1.4% is due to incremental fractures of the composite and accompanying intense deflections of the flags.

which had the lowest and highest strain-to-failure, respectively. High fracture strains (1–2%) were achieved, but the fracture strengths were relatively low. The tensile strength of 30 coupons were evaluated and the average and standard deviation values were 25 and ±8 MPa, respectively.

The $C_{fiber}/PG_{interface}/HfC_{matrix}$ composite was annealed at 2200°C for 4 h in argon. The structural stability was confirmed by the observation that tensile strength for the annealed composites (average 26 and ±6 MPa standard deviation) was the same (within experimental error) as reported above for the as-produced composite. In addition, no obvious structural changes were observed by SEM. As-produced and annealed $C_{fiber}/PG_{interface}/HfC_{matrix}$ composites failed between the plies and not at the interface within the porous HfC region. A portion of $C_{fiber}/PG_{interface}/HfC_{matrix}$ composite remained well adhered on the mounting tabs after testing. The fracture surfaces showed a very rough morphology and extensive fiber pull-out was observed. The porous HfC layer (Fig. 5d), located between the PG layer and the fully dense HfC matrix, presumably provided additional mechanism for crack deflection and enhanced strain-to-failure capability. However, the relative contributions of the porous HfC region and the PG interfacial layer for the strain capability are not known. SEM analysis indicated that the PG interface was the primary region for crack deflection.

The tensile strength of $C_{fiber}/PG_{interface}/HfC_{matrix}$ composite is moderate indicating only a small fraction of the fiber strength was available to carry the load. The SEM analysis was not sufficient to identify the weakening mechanism for the composite. It is possible that further engineering is required for the PG interface coating between the carbon fibers and HfC matrix. The present investigation used Rayon fibers, which may be partly responsible for low tensile strength values. Therefore, additional efforts are necessary to extend the present results to the fabrication of composites with alternate carbon fiber types and weave geometries, such

as 3D woven structures. 3D woven structures could offer higher strength to improve the shear component of the whole composite and hence is expected to increase the mechanical properties in off-axis loading directions. Additional load bearing capability of the composite could possibly be attained by producing very fine and equiaxed grains of HfC matrix phase.

4. Conclusions

A wide range of HfC, TaC and HfC/TaC coating morphologies on graphite and pyrolytic graphite substrates have been studied and correlated with mechanical properties. The coating adherence to the pyrolytic graphite substrate is achieved using deposits of HfC consisting of randomly oriented fine grains near the substrate. An intermediate region (20 to 30 μm) consisting of porous structure form a 'compliant' composite, i.e., a composite with relatively high strain-to-failure. The randomly oriented fine grains grew into large columnar grains and produced dense carbide coatings. Small additions of TaC to the HfC matrix did not result in any obvious change in microstructure compared to HfC samples alone.

The necessary requirement for the toughening has been attained using high-strength carbon fibers and the engineering of the fiber matrix interface. Pyrolytic graphite (PG) as a compliant interface ensured crack deflection and its layered structure was the source of strain energy release through frictional dissipation of crack propagation. Further engineering is necessary to reduce PG layer thickness and increase the strain capability. The tensile strength of $C_{fiber}/PG_{interface}/HfC_{matrix}$ composite was 26 MPa (with standard deviation of 8 MPa). The strain-to-failure values for the $C_{fiber}/PG_{interface}/HfC_{matrix}$ composites were larger than 1% and, in many cases, reached as high as 2%. This strain capability exceeds most ceramic-matrix composites, but the tensile strength values are low. Superior fibers with 3D architecture are expected to increase the load bearing capability of the composite.

Hafnium carbide was thermodynamically stable in the reducing environment upon heating at 2200°C for four hours. This annealing condition did not change the microstructure, no phase transformations or reactions were observed by SEM and no strength degradation occurred. A viable HfC matrix for carbon reinforced composite for aerospace applications must be "prime reliant" (i.e., it must guarantee protection of a component that would not catastrophically fail or oxidize under use conditions). Additional work is necessary to define the oxidation resistance of the $C_{fiber}/PG_{interface}/HfC_{matrix}$ composite for time, temperature and stress regimes in oxidizing environment.

References

1. L. KAUFMAN and H. NESOR, "Stability Characterization of Refractory Materials under High Velocity Atmospheric Flight Conditions," AFML-TR-69-84, Part II, Vol. II: Facilities and Techniques Employed for Cold Gas/Hot Wall Tests, ManLabs, Inc., Cambridge, Mass. (Sept. 1969).
2. *Idem.*, "Stability Characterization of Refractory Materials under High Velocity Atmospheric Flight Conditions," AFML-TR-69-84, Part II, Vol. III: Facilities and Techniques Employed for Cold Gas/Hot Wall Tests, MansLabs, Inc., Cambridge, Mass. (Sept. 1969).
3. *Idem.*, "Stability Characterization of Refractory Materials under High Velocity Atmospheric Flight Conditions," AFML-TR-69-84, Part III, Vol. I: Experimental Results of Low Velocity Cold Gas/Hot Wall Tests, ManLabs, Inc., Cambridge, Mass. (Sept. 1969).
4. R. PERKINS, L. KAUFMAN and H. NESOR, "Stability Characterization of Refractory Materials under High Velocity Atmospheric Flight Conditions," AFML-TR-69-84, Part III, Vol. II: Experimental Results of High Velocity Cold Gas/Hot Wall Tests, ManLabs, Inc., Cambridge, Mass. (Sept. 1969).
5. L. KAUFMAN and H. NESOR, "Stability Characterization of Refractory Materials under High Velocity Atmospheric Flight Conditions," AFML-TR-69-84, Part III, Vol. III: Experimental Results of High Velocity Hot Gas/Cold Wall Tests, ManLabs, Inc., Cambridge, Mass. (Sept. 1969).
6. *Idem.*, "Stability Characterization of Refractory Materials under High Velocity Atmospheric Flight Conditions," AFML-TR-69-84, Part IV, Vol. I: Theoretical Correlation of Material Performance with Stream Conditions, ManLabs, Inc., Cambridge, Mass. (Sept. 1969).
7. J. B. BERKOWITZ-MATTUCK, *J. Electrochem. Soc.* **113**(9) (1966) 908.
8. G. M. MEHROTRA, R. ARUN and M. SUBRAMANIAN, "Oxidation Behavior of Hot Pressed TiC-ZrB_2, TiC-$HfBr_2$, SiB_6-ZrB_2 and SiB_6-HfB_2 Composites," in Thermal Analysis in Metallurgy, edited by R. D. Shull and A. Joshi (The Minerals, Metals & Materials Soc, 1992) p. 346.
9. W. C. TRIPP and H. C. GRAHAM, *J. Electrochem. Soc., Solid State Sci.* **118**(7) (1971) 1195.
10. J. BULL, J. WHITE and L. KAUFMAN, "Ablation Resistant Ziconium and Hafnium Ceramics," US Patent May 12 (1998) Patent No. 5,750,450.
11. A. BRONSON, Y.-T. MA and R. R. MUTSO, *J. Electrochem. Soc.* **139**(11) (1992) 3183.
12. E. V. CLOUGHERTY, R. L. POBER and L. KAUFMANN, *Trans. Metall. Soc. AIME* **242** (1968) 1077.
13. W. C. TRIPP, H. H. DAVIS and H. C. GRAHAM, *Ceram. Bull.* **52**(8) (1973) 612.
14. J. D. BULL, D. J. RASKY and J. C. KARIKA, "Stability Characterization of Diboride Composites Under High Velocity Atmospheric Flight Conditions," 24th Int. SAMPE Techn. Conf., Oct. 20–22, 1992.
15. J. W. HINZE, W. C. TRIPP and H. C. GRAHAM, *J. Electrochem. Soc.; Solid-State Sci. & Techn.* **122**(9) (1975) 1249.
16. M. M. OPEKA, I. G. TALMY, E. J. WUCHINA, J. A. ZAYKOSKI and S. J. CAUSEY, *J. Eur. Ceram. Soc.* **19** (1999) 2405.
17. S. R. LEVINE, E. J. OPILA, M. C. HABIG, J. D. KISER, M. SINGH and J. A. SALEM, *J. Eur. Ceram. Soc.* **22** (2002) 2757.
18. E. J. OPILA and M. J. HALBIG, *Ceram. Eng. & Sci. Proc.* **22**(3) (2001) 221.
19. F. DECKER and C. T. SIMS, in "The Superalloys," edited by C. T. Sims and W. C. Hagel (John Wiley, New York, 1972).
20. E. L. COURTRIGHT, H. C. GRAHAM, A. P. KATZ and R. J. KERANS, "Ultrahigh Temperature Assessment Study Ceramic Matrix Composites," Rpt. No, WL-TR-91-4061, Wright Patterson Air Force Base, OH, 1991.
21. W. B. HILLIG, "Prospects for Ultra-High Temperature Ceramic Composites," in "Tailoring Multiphase and Composite Ceramics," edited by R. E. Tressler, G. L. Messing, C. G. Pantano and R. E. Newnham (Materials Science and Research, 1986) Vol. 20, p. 697.
22. K. UPADHYA, J. M. YANG and W. P. HOFFMANN, *Amer. Ceram. Soc. Bull.* **76**(12) (1997) 51.
23. N. J. SHAW, J. A. DICARLO, N. JACOBSON, S. R. LEVINE, J. A. NESBITT, H. B. PROBST, W. SANDERS and C. A. STEARNS, "Materials for Engine Applications Above 3000°F—an Overview," NASA Techn. Memorandum, 100169 (1987).

24. C. E. WICKS and F. E. BLOCK, "Thermodynamic Properties of 65 Elements—Their Oxides, Halides, Carbides and Nitrides, Bull. No. 605, U.S. Bureau of Mines (1963).
25. H. L. SCHICK, "Thermodynamics of Certain Refractory Compounds" (Academic Press, New York, 1966) Vol. II.
26. G. R. HOLCOMB and G. R. ST. PIERRE, *Oxid. Met.* **40**(1/2) (1993) 109.
27. E. L. COURTRIGHT, J. T. PRATER, G. R. HOLCOMB, G. R. ST. PIERRE and R. A RAPP, *Oxid. Met.* **36** (1991) 42337.
28. D. GOZZI, G. GUZZARDI, M. MONTOZZI and P. L. CIGNINI, *Solid State Ion.* **101–103** (1997) 1243.
29. C. B. BARGERON and R. C. BENSON, "High Temperature Oxidation of Hafnium Carbide," NASA CP-3054, Part 1, NASA (Washington, DC, 1989) p. 69.
30. *Idem.*, *Surf. Coat. Techn.* **36** (1988) 111.
31. C. B. BARGERON, R. C. BENSON, A. N. JETTE and T. E. PHILLIPS, *J. Amer. Ceram. Soc.* **76**(4) (1993) 1040.
32. G. EMIG, G. SCHOCH and O. WORMER, *J. de Physique* **IV**(3) (1993) 535.
33. L. E. TOTH, "Transition Metal Carbides and Nitrides" (Academic Press, New York, 1971).
34. E. K. STORMS, "The Refractory Carbides" (Academic Press, New York, 1967).

Received 9 March 2004
and accepted 20 April 2004